Lasers in Surgery and Medicine 53:1266–1278 (2021)

Characteristics of Non-Ablative Resurfacing of Soft Tissues by Repetitive Er:YAG Laser Pulse Irradiation

Matjaz Lukac,[1]* Anze Zorman,[2] Nejc Lukac,[3] Tadej Perhavec,[4] and Blaz Tasic[3]
[1]*Institut Jozef Stefan, Jamova 39 SI-1000, Ljubljana, Slovenia*
[2]*Medilase Dermatology & Laser Center, Tbilisijska 59 SI-1000, Ljubljana, Slovenia*
[3]*Faculty of Mechanical Engineering, University of Ljubljana, Askerceva 6 SI-1000, Ljubljana, Slovenia*
[4]*Fotona, d.o.o., Stegne 7 SI-1000, Ljubljana, Slovenia*

Background and Objectives: Recently, several minimally invasive gynecological, ENT and esthetic procedures have been introduced that are based on delivering "smooth" sequences of Er:YAG laser pulses to cutaneous or mucosal tissue at moderate cumulative fluences that are not only below the ablation threshold but typically also do not require local anesthesia. To explain the observed clinical results using "smooth-resurfacing," it has been suggested that in addition to the direct heat injury to deeper-lying connective tissues, there is an additional mechanism based on indirect triggering of tissue regeneration through short-exposure, intense heat shocking of epithelia. The goal of this study is to improve understanding of the complex dynamics of the exposure of tissues to a series of short Er:YAG laser pulses, during which the thermal exposure times transition from extremely short to long durations.

Study Design/Materials and Methods: A physical model of laser-tissue interaction was used to calculate the temperature evolution at the irradiated surface and deeper within the tissue, in combination with a chemical model of tissue response based on the recently introduced variable heat shock (VHS) model, which assumes that the tissue damage represents a combined effect of two limiting Arrhenius′ processes, defining cell viability at extremely long and short exposure times. Superficial tissue temperature evolution was measured during smooth-resurfacing of cutaneous and mucosal tissue, and compared with the model. Two modalities of non-ablative resurfacing were explored: a standard "sub-resurfacing" modality with cumulative fluences near the ablation threshold, and the "smooth-resurfacing" modality with fluences below the patient′s pain threshold. An exemplary skin tightening clinical situation was explored by measuring pain tolerance threshold fluences for treatments on abdominal skin with and without topical anesthesia. The obtained temperature data and pain thresholds were then used to study the influence of Er:YAG laser sequence parameters on the superficial (triggering) and deep (coagulative) tissue response.

Results: The simulations show that for the sub-resurfacing modality, the parameter range where no excessive damage to the tissue will occur is very narrow. On the other hand, using pain tolerance as an indicator, the smooth-resurfacing treatments can be performed more safely and without sacrificing the treatment efficacy. Two preferred smooth-resurfacing treatment modalities were identified. One involves using optimally long pulse sequence durations (≈1–3 seconds) with an optimal number of pulses ($N \approx 10$–30), resulting in a maximal short-exposure superficial tissue response and moderate coagulation depths. And for deeper coagulation, without significant superficial heat shocking, very long pulse sequences (>5 seconds) with a large number of delivered pulses are to be used in combination with topical anesthesia.

Conclusions: A comparison of the simulations with the established smooth-resurfacing clinical protocols in gynecology, ENT, and esthetics suggests that, through clinical experience, the clinical protocols have been optimized for the maximal superficial heat shock triggering effect. Further research is needed to gain a better understanding of the proposed role of heat shock triggering in the clinically observed regeneration of cutaneous, vaginal, and oral tissues following Er:YAG laser smooth-resurfacing. Lasers Surg. Med. © 2021 The Authors. *Lasers in Surgery and Medicine* published by Wiley Periodicals LLC.

Key words: Er:YAG laser; non-ablative resurfacing; repetitive irradiation; SMOOTH; variable heat shock; rejuvenation

Conflict of Interest Disclosures: All authors have completed and submitted the ICMJE Form for Disclosure of Potential Conflicts of Interest and have disclosed the following: The authors are affiliated also with Fotona, d.o.o.

*Correspondence to: Matjaž Lukač, PhD, Institut Jozef Stefan, Jamova 39, SI-1000 Ljubljana, Slovenia.
E-mail: matjaz.lukac@fotona.com

Received 8 December 2020; revised 4 February 2021; Accepted 14 March 2021
Published online 1 April 2021 in Wiley Online Library (wileyonlinelibrary.com).
DOI 10.1002/lsm.23402

INTRODUCTION

Ablative skin resurfacing using CO_2 and Er:YAG lasers has proven to be an effective and reproducible method for treating wrinkles [1–4]. Of particular interest has been resurfacing with the Er:YAG laser wavelength ($\lambda = 2940$ nm), as it is positioned at the highest far-infrared water-absorption peak of $\lambda = 2940$ nm. The laser-induced temperature increase ΔT is thus limited to the superficially irradiated tissue layer with its thickness determined by the laser's extremely short optical penetration depth (δ) of 1–3 μm [5–7].

Although ablative laser resurfacing procedures have been found to be extremely effective, a major disadvantage is the erosion of large surfaces, which necessitates a recuperation period of 1–2 weeks. There are also potential risks of infections, scarring, or hyper- and hypo-pigmentation [8–10]. For this reason, it has been proposed to utilize the unique superficial absorption characteristics of Er:YAG also for less invasive, non-ablative treatments [11–16].

As opposed to ablative procedures, the main mechanism of action of non-ablative procedures is based on selective thermal damage followed by new collagen formation [17,18]. The depth of the tissue's thermal response, that is, of the tissue coagulation, is determined by the amount of heat that can be delivered to the tissue in a non-ablative manner. As in the absence of thermal diffusion the ablation threshold fluence F_{abl} (in J/cm^2), is inversely proportional to δ [5,6], the heat energy that can be delivered into the tissue by a single Er:YAG laser pulse is relatively small. This applies especially as the existing Er:YAG laser technology limits single pulse durations to below several milliseconds, limiting the time available for conductive superficial cooling of the tissue during the laser pulse. It is for this reason that non-ablative Er:YAG treatments have been performed by repetitive stacking of sub-threshold Er:YAG laser pulses, resulting in a higher cumulatively delivered sequence fluence, F_s [3,5,11–16].

Initial studies of non-ablative thermal treatments with repetitive stacking of Er:YAG laser pulses were made at cumulative fluences (F_s) close to the ablation threshold [11–16]. This resulted in significant damage to the epidermis, leading to subsequent peeling of the damaged epidermis, making the treatments "delayed ablative" [3]. Therefore, with this type of non-ablative resurfacing, the epithelium is in reality damaged, but not completely removed during the procedure, and acts as a wound dressing [15,16]. For this reason, this type of sub-ablative (or minimally ablative) resurfacing modality can be called also a "sub-resurfacing" modality, analogously to what has been proposed in [18].

More recently, however, excellent clinical results have been reported for procedures using "SMOOTH" mode Er:YAG laser pulse sequences, characterized by moderate cumulative fluences that are not only below the ablation threshold but also below the patient's pain threshold [19–32]. The SMOOTH mode Er:YAG laser energy has been found to induce changes in the deeper skin or mucosa, initiating a process of cell activation, production of extracellular matrix, and tissue remodeling, without causing unwanted direct epithelial ablation [33]. The SMOOTH mode Er:YAG lasers have been, for example, very successfully used for non-ablative laser treatment of vaginal [21–26] and oral tissues [27–32], and as well for skin tightening [19,20].

The expression "resurfacing" generally implies removal of the tissue [17,18]. During ablative resurfacing the tissue is vaporized immediately, while with non-ablative resurfacing the removal occurs later when the epithelial and connective tissue is devitalized and replaced. For example, histological studies of fractional non-ablative resurfacing devices demonstrated the laser-affected tissue to be extruded through the heat-induced channels over the course of several days following the treatment [33,34]. With the less aggressive SMOOTH mode treatments, the delayed tissue replacement process is less evident. However, as has been recently shown for the Er:YAG laser vaginal relaxation treatment, a significant exfoliative effect of superficial and intermediate cells of the vaginal mucosa epithelium occurs following the SMOOTH pulse stacking treatment, with the "peeling" effect taking place over the course of one week [35]. This indicates that subsequent gradual tissue removal is associated also with the less aggressive SMOOTH mode treatment. For this reason, "smooth-resurfacing" will be used to describe this type of treatments.

To explain the observed clinical results using smooth-resurfacing, it has been suggested that other indirect mechanisms in addition to the direct heat injury to the deeper-lying connective tissues may play a role in regeneration and remodeling, including vascular damage, recruitment of inflammatory cells, and release of mediators [36]. An additional indirect triggering of tissue regeneration through short-exposure intense heat shocking of epithelia has been proposed [37], based on stimulating signal transduction processes for transcription factor activation, gene expression, and fibroblast growth, leading to new collagen and extracellular matrix formation [38–41].

The exact contribution of the direct and indirect tissue regeneration mechanisms proposed to be involved in smooth-resurfacing still need to be investigated. In order to shed more light on the non-ablative Er:YAG resurfacing mechanisms, we used a numerical model to analyze the characteristics of Er:YAG sub- and smooth-resurfacing, and examined how the requirement that the treatment is effective yet within the pain tolerance may influence the choice of optimal laser treatment parameters. Superficial tissue temperature evolution was measured during smooth-resurfacing of skin and oral mucosa, and compared with the model. An exemplary skin tightening clinical situation was explored by measuring pain threshold fluences for treatments on abdominal skin with and without topical anesthesia. The obtained temperature data and pain thresholds were then used to study the characteristics of the short- and long-exposure's tissue response believed to be

respectively involved in the indirect and direct soft-tissue regeneration mechanisms [19,20,37].

MATERIALS AND METHODS

Physical Model of Resurfacing

A numerical model was applied to the physical process of sub- and smooth-resurfacing of soft tissues, such as skin and mucosa, as originally developed to study thermo-mechanical ablation with mid-IR lasers. The details of the model are described in [7], and will not be repeated here.

In the model, a single wavelength (λ) pulsed laser radiation is delivered to the surface of the treated tissue with a pulse fluence F_p (in J/cm^2). The tissue is modeled as a water-containing homogeneous media characterized by a single absorption coefficient of $k = 1/\delta$ for the delivered laser wavelength λ. For simplicity, a square-shaped laser pulse with duration t_p was assumed. Since the focus of our study was on the Er:YAG laser wavelength with a short penetration depth, the effects of the scattering of the laser light within the tissue were not included. Similarly, it was taken that the laser spot size is much larger than the penetration depth (δ). Therefore, with an exception described in the discussion section, the diffusion of dissipated heat was treated in one dimension using a finite-difference scheme. In all our calculations, we used the physical parameters of the irradiated media as published in Reference [7].

As we were interested in determining at what individual pulse fluence (F_p) and total sequence fluence (F_s) the laser-tissue interaction starts being ablative, the model also included the microscopic physical model of the ablative micro-explosion process, which combines the thermodynamic behavior of tissue water with the elastic response of the solid tissue components [7].

The model was applied to calculate temporal and spatial temperature profiles for single pulses and as well for pulse sequences, each consisting of N consecutive Er:YAG laser pulses with individual (F_p) and cumulative (F_s) fluences, separated by a pulse separation time t_{sep}. The effective duration of the modeled pulse sequences was defined by the sequence duration $t_s = N \times t_{sep}$.

Figure 1 presents a typical temporal profile of the tissue surface temperature during a pulse sequence and the resulting spatial profile within the tissue depth (z) by the end of the sequence.

A multiple pulse train sequence results in N high-temperature peaks ($T_{max\text{-}i}$) that rapidly relax deeper into the tissue by fast thermal diffusion driven by the large temperature gradient over the short optical absorption length. During the pulse sequence, the superficially laser-generated heat is thus being "pumped" by diffusion away from the epithelia, up to several hundred microns deep into the connective tissue (see Fig. 1b). The final, longer persisting surface temperature is in Figure 1 represented by the sequence temperature T_s.

Chemical Model of Non-Ablative Resurfacing

Typically, the tissue damage response is calculated using the Arrhenius damage integral Ω that is for the thermal exposure to a constant elevated temperature T during the thermal exposure time (t_{exp}) equal to [42–45]:

$$\Omega = A \exp(-E/RT) \times t_{exp} \quad (1)$$

Here, A is the frequency factor, that is, the damage rate (in s^{-1}), E is the activation energy (in J/kmol), and R is the gas constant ($R = 8.31\ 10^3$ J/kmol K). The critical (i.e., damage threshold) temperature (T_{crit}), is then typically defined as [42]

$$T_{crit} = E/(R \ln(At_{exp})) \quad (2)$$

In the standard model originally proposed by Henriques and Moritz [44,45], based on measurements for $t_{exp} > 1$ second, it is assumed that a single chemical process representing the kinetics of protein denaturation is involved, and therefore that the Arrhenius coefficients E and A are fixed and independent of the exposure time. However, with more recent studies performed at extremely short exposure times ($t_{exp} < 10$ milliseconds), the obtained activation energies were significantly smaller and the damage threshold temperatures were significantly higher than what would be expected from the standard single process Arrhenius model [37,46–48]. This finding is of particular significance for Er:YAG laser sub-surfacing and smooth-surfacing resurfacing procedures, during which

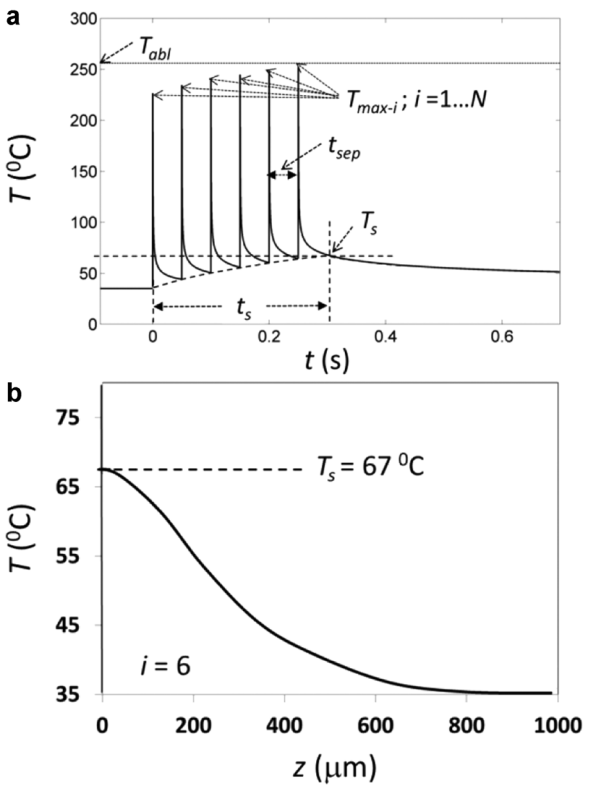

Fig. 1. Exemplary temporal (**a**) and spatial (**b**) temperature profile during and following a laser pulse train (with $N = 6$ and $t_{sep} = 50$ milliseconds). The spatial profile at time $t = t_s$ is presented.

the superficial tissue's thermal exposure transitions from intense, extremely short periods of exposure to peak temperatures $T_{\text{max-}i}$, to long-duration periods of exposure to moderate temperatures for $t > t_s$ (see Fig. 1).

Recently [37], it was demonstrated using a variable heat shock (VHS) model that the observed dependence of the critical temperature on the thermal exposure time can be described as a combined effect of two limiting Arrhenius' processes, defining cell viability at extremely long and short exposure times (see Fig. 2).

The VHS model that was used also in this study assumes that the effective damage integral Ω can be calculated for any exposure from the combined effect of the damage integrals $\Omega_{\text{long}}(t_{\text{exp}})$ and Ω_{short} (t_{exp}) belonging respectively to the long and short Arrhenius processes (see Fig. 2), as follows [37]:

$$(1/\Omega)^p = (1/\Omega_{\text{long}})^p + (1/\Omega_{\text{short}})^p \tag{3}$$

where p is the transition coefficient that determines the transition between the two limiting biochemical processes. The details of the VHS model are described in [37], and will not be repeated here. In this study, the same Arrhenius parameters and the transition coefficient were used as obtained in Reference [37] by fitting Equation (3) to published experimental data: $A_{\text{long}} = 4.7 \times 10^{89}\ \text{s}^{-1}$ and $E_{\text{long}} = 5.67 \times 10^8\ \text{Jkmol}^{-1}$ for the long exposure process, and $A_{\text{short}} = 1.45 \times 10^4\ \text{s}^{-1}$ and $E_{\text{short}} = 1.03 \times 10^7\ \text{Jkmol}^{-1}$ for the short exposure process, and $P = 0.16$ for the transition coefficient. Figure 2 represents the dependence of T_{crit} on the exposure time as calculated based on these parameters.

During an Er:YAG laser pulse sequence, the laser-generated heat dynamics exhibits two phenomena: (i) intense short-duration thermal pulses resulting from individual laser pulses i, with peak temperatures ($T_{\text{max-}i}$) at the surface that may exceed 200°C (see Fig. 1a) [49], biochemically directly affecting only the approximately 10 μm deep superficial tissue layer [37]; and (ii) a slow gradual build-up of the spatial temperature distribution over the total duration of the sequence, extending several hundred microns deep into the tissue, with the surface temperatures (T_s) typically below 50–70°C (see Fig. 1b). According to the VHS model, the first and second phenomena are governed predominantly by the short-exposure and long-exposure Arrhenius' biochemical processes (see Fig. 2), respectively.

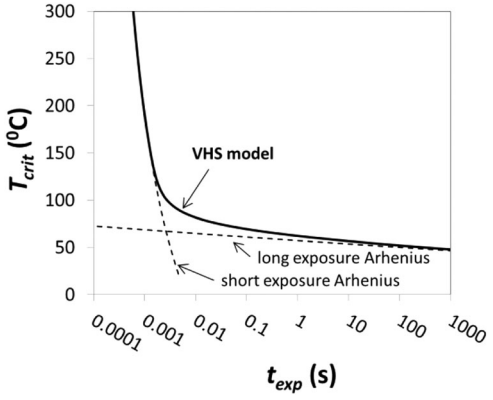

Fig. 2. The variable heat shock (VHS) model's critical temperature as a function of the exposure time. According to the VHS model, the critical temperature represents a combined effect of two limiting Arrhenius' processes, defining cell viability at extremely long and short exposure times [12].

For calculating the cumulative short-pulse Arrhenius process damage to the superficial tissue located at $z = 0$, following a series of $i = 1 \ldots N$, intense short-duration thermal exposures to $T_{\text{max-}i}$, the following probability-summation model of Menendez et al. [50] was used. In this model, it is assumed that the response to each pulse of a multiple-pulse exposure is independent of the response to other pulses; that is, previous pulses do not "sensitize" the tissue to subsequent pulses. The probability P_i for tissue damage response caused by each pulse, $i = 1 \ldots N$ is then obtained from [42]:

$$P_i = 1 - \exp(-\Omega_i) \tag{4}$$

where Ω_i is calculated using Equation (3), assuming exposure to a constant temperature $T_{\text{max-}i}$ for an effective duration t_{eff}. The effective duration was approximated by $t_{\text{eff}} \approx 0.25$ milliseconds, based on results of simulations in [37], assuming $t_p = 0.3$ milliseconds, and represented the duration of an imaginary rectangular temperature pulse of a constant average temperature $T_{\text{max-}i}$, which produces approximately the same amount of damage as the actual "triangularly" shaped temperature pulse. The cumulative "sequence" probability $P_s(N)$ of inducing thermal damage to the tissue surface during N pulses was then calculated using [50,51]:

$$P_s(N) = 1 - (1 - P_1)(1 - P_2) \ldots 1 - P_N \tag{5}$$

that results using $P_s = 1 - \exp(-\Omega_0)$ (see Equation 4), in the cumulative damage integral $\Omega_0(N)$ to the tissue at $z = 0$, as

$$\Omega_0(N) = \text{Ln}(1/(1 - P_s(N))) \tag{6}$$

It has been shown that the superficial tissue damage caused by a single Er:YAG laser pulse is governed mainly by the short-pulse Arrhenius process, and extends about $z \approx 20$ μm deep into the tissue [37]. The average thermal damage ($\Omega_s(N)$) within this thin superficial layer, extending from $z = 0$ to $z = 20$ μm was approximated by $\Omega_s(N) \approx 0.5\ \Omega_0(N)$.

It is to be noted that although the peak temperatures ($T_{\text{max-}i}$) were calculated taking into account the gradual temperature increase during the pulse sequence, the superficial damage $\Omega_s(N)$ does not include the longer exposure tissue response resulting from the gradual temperature build-up and slow decay back to the initial temperature. The damage integral $\Omega(z)$ extending deeper into the tissue, characterized predominantly by the long-pulse exposure process, was calculated separately using the algorithm developed for calculating tissue damage for temporally non-square-shaped thermal exposure pulses [37].

Heat-Pain Threshold Measurement

For all *in-vivo* measurements, informed consent was obtained from all patients and the procedures were performed according to the Declaration of Helsinki. The irradiation procedure used in this study has been cleared for use in the EU according to MDD 93/42 EC-MEDDEV 2.7/1, and is as such regularly applied to treat patients. The imaging study was approved by the Slovenian national ethics committee (application no. 111/02/12).

In order to determine the heat-pain threshold (HPT) for different smooth-resurfacing conditions, 15 patients (mean age 41.5 ± 10.8), eight females and seven males participated in the study on a voluntary basis. Testing took place in a quiet room. Temperature in the room was maintained at 23 ± 1°C. The patients were laid down on a comfortable dermatological bed. In order to get accustomed to different levels of discomfort, each patient underwent an initial "training" procedure at a practice site on the abdomen before the actual measurement on a different abdominal area was performed. The patients were instructed to identify the "pain threshold fluence" above which the patient would not want to be treated. The pain threshold fluence values obtained during the practice were not used in the study.

Thermal stimuli were delivered using an Er:YAG laser (Dynamis SP, manufactured by Fotona d.o.o., Ljubljana, Slovenia) operating in a V-SMOOTH pulse mode. Sequences with pulse separation times $t_{sep} = 25$, 100, and 125 milliseconds were applied, with pulse numbers up to $N = 36$. The laser pulse duration was equal to $t_p = 0.3$ milliseconds. The laser energy was delivered to the abdominal skin area using a T-Runner scanning handpiece (manufactured by Fotona d.o.o.) with a single full-beam spot size of $2r = 9$ mm, scanned over a scanning area consisting of 3×3 spots. Heat-pain thresholds were obtained for treatments without and with topical anesthesia (application of EMLA 25 minutes before the test).

A method of limits was used [52–55], where the laser fluence was gradually increased for each successive scan in steps of $0.2\,J/cm^2$ from a low level until the patient characterized the treatment discomfort as unacceptable. The pain threshold represented the fluence just below this value. Each scan was performed on a previously not-yet-irradiated abdominal skin area, additionally alternating between the left and right half of the abdomen.

Tissue Surface Temperature Measurement

Measurements of the tissue surface temperature evolution as a result of Er:YAG laser irradiation were made on the abdominal skin and intraorally on the inside of the cheeks of the authors using the Dynamis SP laser system (manufactured by Fotona d.o.o.) operating in SP pulse duration mode ($t_p = 0.3$ milliseconds). A thermal camera (ThermaCAM P45, manufactured by FLIR Systems, Inc., Wilsonville, USA) with a frame rate of 50 Hz was used. Two laser handpieces were used: (i) a full-beam handpiece (Fotona R11) and (ii) a patterned-beam handpiece (Fotona PS03), with both handpieces set to a 7 mm spot size. The Fotona PS03 handpiece is equipped with a pixel screen, resulting in the overall laser spot having a patterned (dotted) internal beam structure, with the centers of the individual circular beam dots of diameter of $2r = 0.85$ mm being separated by approximately 2 mm [21]. The motivation behind the design of the patterned PS03 handpiece is to make the treatment less invasive by reducing the treatment area to isolated beam islands [21].

RESULTS

Pain Threshold Fluence

Figure 3a shows the dependence of the pain threshold fluence F_p on pulse sequence duration t_s, as obtained for treatments without topical anesthesia on 15 patients for four pulse sequence settings: (i) $N = 6$, $t_s = 150$ milliseconds; (ii) $N = 30$, $t_s = 3750$ milliseconds; (iii) $N = 36$, $t_s = 3600$ milliseconds; and (iv) $N = 36$, $t_s = 4500$ milliseconds. The above range of studied pulse sequence parameters was chosen based on the practical consideration of the capabilities of currently available Er:YAG laser sources, and acceptable treatment durations.

The influence of the use of topical anesthesia is shown in Figure 3b that depicts the difference in reported pain threshold fluences for two sequence durations (150 and 4500 milliseconds), depending on whether topical anesthesia (EMLA cream) was used or not.

As can be concluded from Figure 3, while pain thresholds vary from patient to patient, the pain threshold fluence is generally higher for longer sequence duration t_s, This can be seen in Figure 4 that shows the dependence of the pain threshold fluence shown in Figure 3 (averaged over 15 patients) on t_s. The additional data points for $t_s = 300$, 1500, and 3900 milliseconds were obtained in a separate experiment on a group of five patients.

Pulse Sequence Temperature

Simulations for full beam (i.e., R11 handpiece) treatments using parameters for cutaneous tissue [7], show that for fluences below the ablation threshold, the sequence temperature increase $\Delta T_s = T_s - T_0$, is linearly dependent on F_s:

$$\Delta T_s \approx \eta_s \times F_s \tag{7}$$

where $\eta_s = \Delta T_s / F_s$. is the sequence temperature slope for a particular set of sequence parameters. While the dependence of the sequence temperature slope on the single-pulse duration (t_p) or on the number of pulses N is relatively small, the dependence of the slope η_s (in units of °C cm^2/J) on the sequence duration t_s (in milliseconds), as obtained by fitting the numerical results to a power function, was found to be well described by ($R^2 = 0.98$):

$$\eta_s = A_s\, t_s^{Ks} \tag{8}$$

Here, the coefficients for the full-beam treatments of cutaneous tissue are $A_s = 84$ and $K_s = -0.43$. Using these parameters, the numerically predicted dependence of η_s on t_s is in Figure 5 represented by a full line. As can be

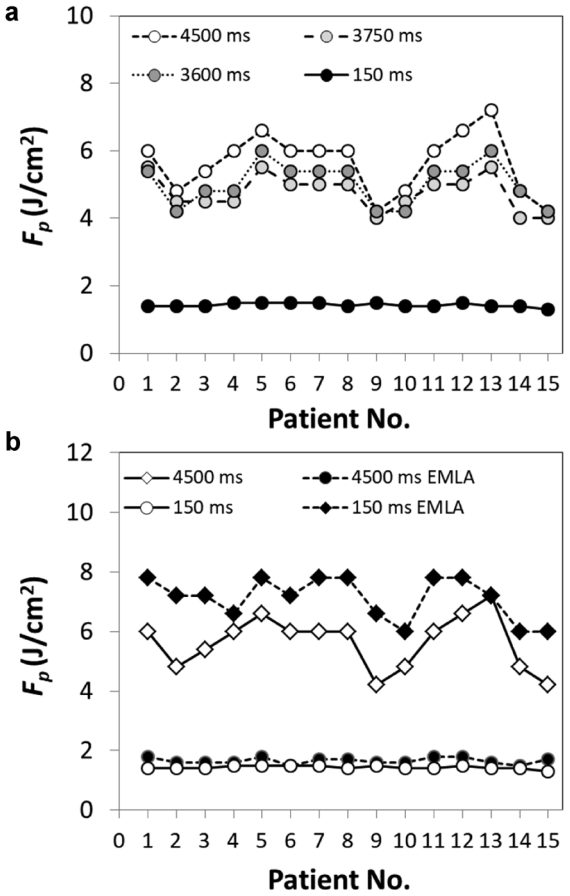

Fig. 3. Measured pain tolerance threshold fluences F_p as obtained on 15 patients for (**a**) sequence durations $t_s = 150$, 3600, 3750, and 4500 milliseconds without topical anesthesia; (**b**) sequence durations $t_s = 150$ milliseconds (circles) and 4500 milliseconds (diamonds) with (closed symbols) and without (open symbols) topical anesthesia.

seen from Figure 5, the simulated dependence is in good agreement with the slopes as measured for the full-beam treatment of the abdominal skin (depicted by full circles).

For comparison, Figure 5 shows the measured slopes for the full-beam treatment of oral and vaginal mucosa, and as well the slopes as measured for cutaneous and mucosal tissues using a patterned handpiece (Fotona PS03). The experimental conditions for the vaginal data [21], were the same as used in this study. The additional skin data point is based on a published ex-vivo skin study [14], using the following experimental conditions: full-beam spot size of 5 mm, $N = 11$, $t_s = 270$ milliseconds, and $F_s = 4.2$ J/cm^2.

The dotted lines represent fits ($R^2 > 0.98$) of the experimental data to Equation (8), with the coefficients $K_s = -0.43$, and $A_s = 69$ for the full-beam treatment of mucosa, $A_s = 28$ for the patterned beam treatment of skin, and $A_s = 18$ for the patterned beam treatment of mucosa.

The reduction of the temperature slope with the duration of irradiation ($\eta \propto t_s^{-0.43}$) can be explained by the increased tissue volume that is heated up within the

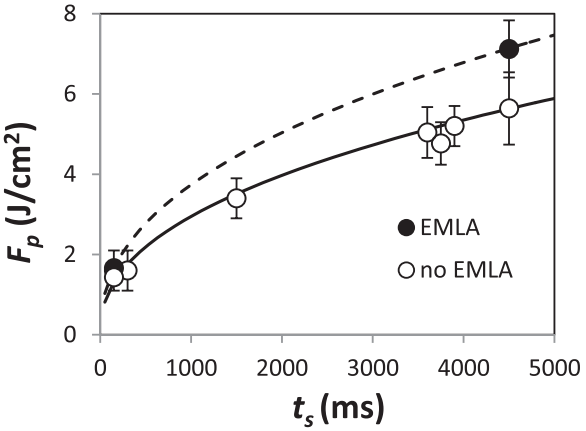

Fig. 4. Dependence of the measured pain threshold fluence F_p, on sequence duration t_s, for treatments with (closed symbols) and without (open symbols) topical anesthesia. The lines represent calculated pain thresholds according to Equation (7), with $\Delta T_p = 12.7$°C for the treatment without (full line), and $\Delta T_{p\text{-EMLA}} = 16.1$°C for the treatment with topical anesthesia (dashed line).

approximate characteristic thermal diffusion depth $x_d \propto t^{0.5}$ [6,7], to which the tissue temperature is affected after a time interval t.

The difference between coefficients for skin and mucosa is tentatively attributed to the fact that the moist mucous tissue requires slightly more energy than the dry skin to be heated up. The lower coefficients for the patterned handpiece as compared with coefficients for the full-beam handpiece are attributed to the radial heat diffusion away from the microspots, in addition to the heat diffusion deeper into the tissue.

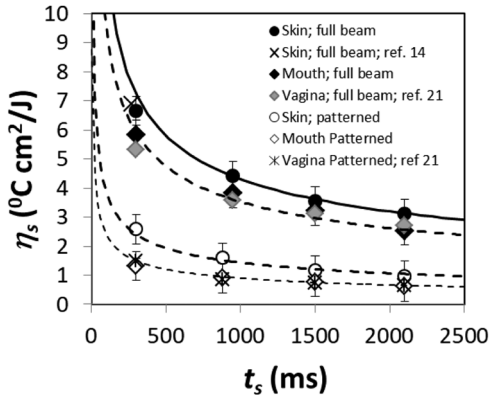

Fig. 5. Simulated temperature slope (full line) for full-beam skin treatments, together with the measured data (full circles). The cross represents the slope obtained from the published experimental data in [14]. For comparison, temperature slopes for full-beam treatments as measured for oral mucosa (closed diamonds), and as published for vaginal mucosa (gray diamonds) [21], are also shown. Additionally, temperature slopes for treatments with a patterned beam (handpiece PS03) are shown as measured on skin (open circles) and intraorally (open diamonds), together with the published data for patterned irradiation of vaginal introitus (asterisk) [21]. The dotted lines represent fits of the experimental data to Equation (8).

Pain Threshold Temperature

The obtained dependence of ΔT_s on the laser fluence F_s for different sequence durations t_s (Equations 7 and 8), enables the calculation of the sequence temperature elevations ΔT_s corresponding to the measured pain threshold fluences. The resulting calculated pain threshold temperature elevations (ΔT_p) as shown in Figure 6 are approximately constant across a wide range of sequence durations, demonstrating also that the pain threshold temperature is not significantly affected by the number of pulses N or maximal temperatures $T_{max\text{-}i}$. On average, the pain threshold temperature increase is equal to $\Delta T_p = 12.7 \pm 2.0$°C for treatments without topical anesthesia, and to $\Delta T_{p\text{-}EMLA} = 16.1 \pm 1.6$°C for treatments with topical anesthesia.

Deep Tissue Response

Figure 7a shows the calculated long-exposure coagulation depths (z_c) as a function of the sequence duration t_s, for three sub-ablative sequence fluences, $F_s = 2.4$, 4.8, and 7.2 J/cm^2, and three pulse separation times $t_{sep} = 25$, 75, and 125 milliseconds. The tissue coagulation depth (z_c) is defined as the tissue depth below which the cell injury Ω (z) is smaller than $\Omega = 0.5$ [7], in agreement with the finding that the value of damage integral of $\Omega \approx 0.5$ defines the threshold below which the skin damage can be tolerated without the occurrence of irreversible epidermal injury [44,45].

As can be concluded from Figure 7, the coagulation depth depends predominantly on cumulative fluence F_s and t_s while the internal pulse sequence structure characterized by N and t_{sep}, is relatively unimportant. This is demonstrated by showing both, the symbol and trend line, where the same trend line applies for different pulse separations t_{sep} (represented by different symbols), and consequently also for different N.

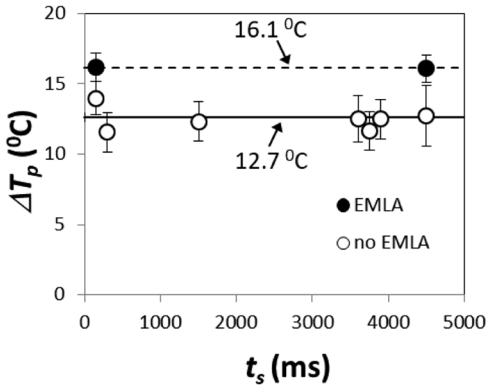

Fig. 6. Dependence of the pain threshold temperature elevation ΔT_p (open symbols) and $\Delta T_{p\text{-}EMLA}$ (closed symbols) on the sequence duration. The full line represents the average pain threshold temperature increase for abdominal skin treatments without anesthesia, $\Delta T_p = 12.7$°C, and the dashed line represents the average pain threshold temperature increase for abdominal skin treatments with anesthesia, $\Delta T_{p\text{-}EMLA} = 16.1$°C.

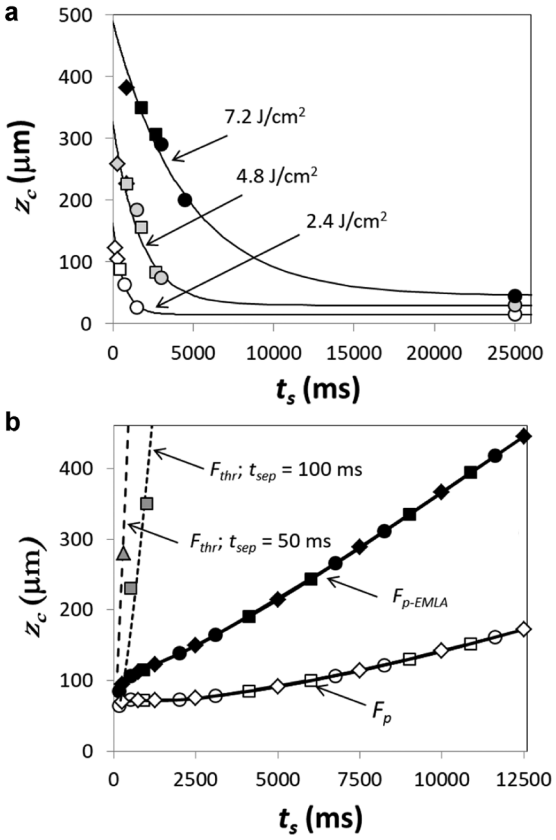

Fig. 7. (**a**) Calculated coagulation depths (z_c) for three non-ablative sequence fluences $F_s = 2.4$, 4.8, and 7.2 J/cm^2, as a function of the sequence duration t_s, for $t_{sep} = 25$ milliseconds (diamonds), 75 milliseconds (squares), and 125 milliseconds (circles). The lines are a visual guide for the eye; (**b**) Full lines represent calculated coagulation depths for different sequence durations at corresponding pain threshold fluences for without (F_p) and with topical anesthesia ($F_{p\text{-}EMLA}$), for t_{sep} of 25 milliseconds (diamonds), 75 milliseconds (squares), and 125 milliseconds (circles). Dashed lines represent calculated coagulation depths for ablation threshold fluences for $t_{sep} = 100$ and 50 milliseconds. Published measured coagulation depths are represented by the gray squares [19] and the gray triangle [23].

It is important to note that heat diffusion does not last only for the duration of the sequence (t_s) but continues also after the sequence has ended. Therefore the total "duration" of heat diffusion is the same for all sequence durations. In Figure 7a, the observation that longer sequence durations give lower coagulation depths is a consequence of lower surface temperatures (T_s) for longer t_s (see Equation 8), resulting also in smaller damage integrals (see Equation 1).

In Figure 7b, the coagulation depths increase with sequence duration because the sequence fluence is for each t_s adjusted to be equal to either the pain threshold fluence F_p or $F_{p\text{-}EMLA}$ (representing smooth-resurfacing conditions) or to the ablation threshold fluence F_{thr} (representing sub-surfacing conditions), corresponding to that sequence duration. Since both, the pain and ablation threshold fluences are higher for longer t_s, more laser

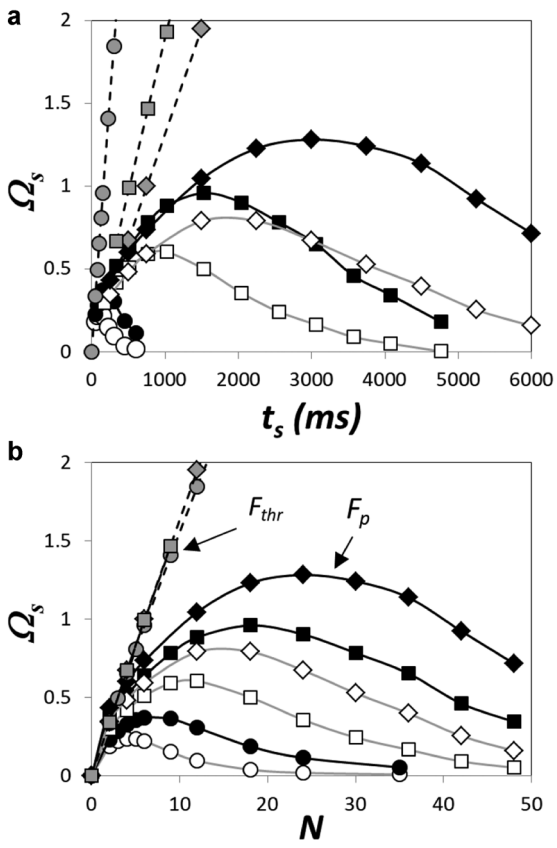

Fig. 8. Calculated short-exposure superficial damage for sub-resurfacing (gray symbols connected by dashed lines) and smooth-resurfacing (black and open symbols connected by full lines), as a function of the sequence duration t_s (**a**) or the number of pulses N (**b**). Black and open symbols represent smooth-resurfacing with and without topical anesthesia, respectively. The calculated damage integrals are for pulse separation times t_{sep} of 25milliseconds (diamonds), 85 milliseconds (squares), and 125 milliseconds (circles).

energy can be delivered with longer t_s, resulting in deeper coagulation depths (z_c).

The pain threshold fluences were calculated using Equation (7) for treatments without (F_p) or with topical anesthesia, taking $\Delta T_p = 12.7°C$ or $\Delta T_{p\text{-EMLA}} = 16.1°C$, correspondingly. As can be concluded from Figure 8b (full lines), smooth-resurfacing can result in significant coagulation depths, providing that appropriately long sequence durations t_s are used, allowing sufficiently high yet still tolerable sequence fluences F_s.

The coagulation depths at the "smooth" fluences, i.e., at the fluences just below the pain threshold, do not depend on N or t_{sep}, On the other hand, during sub-resurfacing at least a partial or delayed epidermal ablation occurs, and the coagulation depth depends not only on t_{sep} but also on the single pulse duration t_p [7]. Two examples of sub-resurfacing are in Figure 7b shown with dashed lines, and represent coagulation depths at corresponding ablation threshold fluences F_{thr}, for $t_{sep} = 100$ milliseconds and $t_p = 0.25$ milliseconds, and for $t_{sep} = 50$ milliseconds and $t_p = 0.55$ milliseconds.

For comparison, Figure 7b also shows published coagulation depths as observed following "standard" sub-resurfacing treatments. The gray squares represent coagulation depths as measured on histologic samples of rat skin treated by an Er:YAG laser, with $t_{sep} = 100$ milliseconds, and $t_s = 500$ or 1000 milliseconds [19]. Similarly, the gray triangle represents the published depth of dermal regeneration as histologically observed on human eyelid skin following treatment with an Er:YAG laser, with $t_{sep} = 50$ milliseconds, and $t_s = 300$ milliseconds [23].

Superficial Tissue Response

Figure 8 shows the calculated superficial damage (Ω_s) for different sub- and smooth-resurfacing parameters, as calculated using Equation (6). Similarly to the calculation of the coagulation depths, the cumulative fluence was for any pulse sequence parameter combination set to be equal to either the ablation threshold fluence (representing sub-surfacing conditions), or to the pain tolerance threshold fluence, representing smooth-resurfacing conditions.

As can be seen from Figures 8a and b, as opposed to the deep tissue response, the superficial damage depends not only on the sequence duration but also on the number of pulses N. This is as expected since the superficial tissue response is a consequence of the high-temperature peaks ($T_{max\text{-}i}$), and therefore it is not the same whether the cumulative fluence is distributed among a small number of high-intensity peaks, or among a large number of smaller intensity peaks.

As can be seen from Figure 8, using the smooth-resurfacing technique represents a significant advantage over sub-surfacing since the damage can be limited to a maximal level defined by the number of pulses N and pulse separation time t_{sep}. On the other hand, the cumulative short-exposure damage during sub-resurfacing grows approximately linearly with N and t_{sep}.

DISCUSSION

In this study, characteristics of non-ablative resurfacing of soft tissues by repetitive Er:YAG laser pulse irradiation were analyzed for the first time from the viewpoint of the maximal fluences deliverable in a clinical setting, as determined by the patients' pain threshold. Additionally, using the VHS [12], and probability-summation model [50], the dependence of the proposed superficial heat shock triggering effects on parameters of the non-ablative Er:YAG laser resurfacing were studied as well. Attention was focused on the difference between the standard, "sub-resurfacing" pulse stacking technique, with Er:YAG laser fluences close to the ablation threshold (F_{thr}), and the "smooth-resurfacing" technique, characterized by moderate fluences ($F_s \le F_p$, $F_{p\text{-EMLA}}$) with resulting tissue temperatures below the heat pain tolerance threshold (HPT).

The published cutaneous HPT temperatures (T_{HPT}) for several-seconds-long exposures are for different body

areas in the range of 41–52°C [52–54], in rough agreement with the pain threshold temperature for smooth-resurfacing of abdominal skin of $T_p \approx 48$°C, as found in this study. In agreement with the VHS model and the assumption that the pain threshold is related to the risk of irreversible damage, the HPT has been observed to increase toward shorter exposures, and was reported to be equal to $T_{HPT} \approx 58$°C for $t_{exp} \approx 0.3$ seconds and to $T_{HPT} \approx 75$°C for $t_{exp} \approx 0.05$ seconds [55]. Similar heat pain thresholds have also been obtained for oral mucosa, with $T_{HPT} \approx 48$°C for long exposures [56], and $T_{HPT} \approx 65$–70°C for approximately 0.1 seconds long exposures [57].

On a long temporal scale, the overall thermal effect of a $\Delta t = t_s$ long sequence of short Er:YAG laser pulses is to heat up the tissue approximately to the same temperatures as if the laser energy was delivered to the tissue in a single $t_p = t_s$ long pulse with the same pulse fluence as delivered during the sequence ($F_p = F_s$). Additionally, as the Er:YAG laser wavelength is limited to its very shallow optical penetration depth, it has been hypothesized that instead of having to rely on the pulse sequence heat-pumping technique, devices with a deeper penetration depth and longer pulse durations may represent a more suitable means for deep thermal remodeling [58]. However, the published clinical results using the smooth-resurfacing technique [19–32], suggest that the superficial heat shocking resulting from individual short laser pulses within a SMOOTH sequence may represent an additional, indirect mechanism of action for regenerating epithelial and deeper-lying connective tissues [36–41,58–67], which is complementary to the conventional direct slow stimulation of fibroblasts [68].

The superficial heat shocking resembles the effects of the micro-needling technique, which aims not to injure keratinocytes but to stimulate them with superficial punctures and without any injury to fibroblasts [69,70]. The smooth-resurfacing laser-induced thermal triggering mechanism can be viewed as non-ablative thermal "needling" (i.e., triggering) of the total treated skin surface, with the action of the spatially sharp needles being replaced by the action of temporarily "sharp" but spatially extended heat shock pulses. In this study, the level of superficial heat shock triggering was evaluated by assuming that the level of thermal "needling" is related to the superficial damage resulting from the multiple short-duration exposures.

Based on Figures 7b and 8, it can be concluded that for smooth-resurfacing there are two optimal treatment regimes. When a maximal heat shock triggering effect, with optimal short exposure damage Ω, and moderate coagulation depths of about 100 μm are desired, the optimal sequence durations and the number of pulses are in the range up of about $t_s = 1$–3 seconds (see Fig. 8a) and $N = 12$–30 pulses (see Fig. 8b). And when deeper coagulation depths are to be achieved, then long sequence durations of about $t_s = 5$–10 seconds (see Fig. 7b), consisting of a large number of pulses of about $N = 80$–50, are to be used. Under these deep coagulation conditions, the heat shock triggering effect is extremely small, typically below $\Omega = 0.001$.

It may be interesting to analyze, using the findings of this study, the three clinical areas where smooth-resurfacing treatments are most commonly being performed, apart from skin tightening: gynecology, ENT, and intra-oral esthetics. These treatments consist of non-ablative resurfacing of the mucosal tissue to thermally initiate a process of cell activation, production of extracellular matrix, and tissue remodeling that continues up to 6 months following treatment [22,36]. The treated mucosa undergoes rejuvenation consisting of an increase in epithelial thickness, fibroblast proliferation, an increase in the amount of collagen, and vascularization [36], resulting in improved tissue tightness and elasticity. The rejuvenation effects of the minimally invasive smooth-resurfacing procedure, which represents an alternative to more aggressive and risky surgical procedures, are temporary, lasting for up to several years, after which an additional touch-up procedure may be needed. In gynecology, tissue rejuvenation results in an alleviation of symptoms of genitourinary syndrome of menopause (GSM), stress urinary incontinence, and vaginal relaxation syndrome [21–26,36]. In ENT, non-ablative resurfacing of soft palate, uvula, and tonsillary regions has been reported to significantly reduce symptoms of chronic snoring-related sleep disorders [29–32]. And in esthetics, the intraoral smooth-resurfacing has been demonstrated to represent a safe, painless, and effective treatment option for accentuated nasolabial folds (NLFs) wrinkles [27,28].

The following clinical protocols are most commonly used for smooth-resurfacing of oral and vaginal mucosa [21–32]: (a) full-beam handpiece protocol with $t_s \approx 2100$ milliseconds, $N = 24$ pulses and $F_s = 12$ J/cm^2, (b) patterned handpiece protocol with $t_s \approx 2100$ milliseconds, $N = 24$ pulses, and $F_s = 24$ J/cm^2; or (c) patterned handpiece protocol with $t_s \approx 950$ milliseconds, $N = 12$ pulses, and $F_s = 20$ J/cm^2. Using the sequence temperature slopes reported in this study (see Fig. 4) to calculate treatment temperatures T_s associated with these three protocols, we obtain $T_s \approx 65$°C, 51°C, and 54°C for protocols a, b and c, respectively. The temperatures achieved with protocols (b) and (c) are close to the pain thresholds as measured in other mucous tissues [56]. For this reason, practitioners often decide to administer topical anesthesia. The protocol (a) where higher sequence temperatures are achieved is performed only deeper in the vagina where vaginal innervation is lower [71]. An exception is the vaginal atrophy protocol where lower laser parameters are used, and the mucosa is warmed up to only some 45°C [23]. Similarly, for irradiations in more sensitive areas such as of the vaginal vestibule the fluence of the protocol (b) is reduced to $F_s = 12$ J/cm^2 ($T_s \approx 43$°C) [21].

It is interesting to note that the established clinical smooth-resurfacing treatment protocols for mucosa consist of $N = 12$-24 Er:YAG pulses delivered during $t_s =$ 950–2100 milliseconds at an average separation time of $t_{sep} \approx 85$ milliseconds, in rough agreement with the

predicted optimal t_s and N for superficial triggering (see Fig. 8).

Furthermore, our analysis also provides a potential explanation for why smooth-resurfacing clinical protocols almost in all cases include treatments using a patterned handpiece. Namely, with patterned handpieces, the irradiated tissue does not cool down only by the heat diffusion deeper into the tissue but also by the heat diffusion in the radial direction away from the irradiated microspots. This cooling mechanism is more effective during the long sequence duration (t_s) than during the short duration temperature peaks. For this reason, the final sequence temperature (T_s) is more significantly reduced than the temperature peaks $T_{max\text{-}i}$. As can be seen from Figure 5, the temperature slope coefficient A_s is for a patterned handpiece by a factor of 3–4 smaller as compared with the slope for the full-beam handpiece (see Equation 7). This means that three to four times higher cumulative fluences (F_s) can be delivered without exceeding the pain tolerance threshold temperature. On the other hand, as the radial heat diffusion has a smaller effect on the high-temperature peaks ($T_{max\text{-}i}$), the higher cumulative fluence will for the same level of deep tissue coagulation result in an increased level of superficial triggering. Therefore, patterned handpieces are generally better suited for the maximal heat shock triggering effect compared with full-beam handpieces.

To demonstrate the influence of radial heat diffusion for small diameter beam sizes we carried out a limited numerical analysis using a 3D cylindrical coordinate system model. The resulting temporal profiles of the skin surface temperature during a sequence with $N = 24$ micro pulses, delivered by a full beam ((R11 with 7 mm spot size) or by a patterned beam handpiece (PS03 with 0.85 mm micro spot size) are shown in Figure 9.

As can be seen from Figure 9, for the same final sequence temperature ($T_s = 50°C$) (and resulting deep tissue response), the high-temperature peaks ($T_{max\text{-}i}$) are approximately 30% higher for the patterned handpiece. A damage integral calculation using Equations (5) and (6) shows that this difference results in two times stronger (in terms of Ω_s) patterned thermal "needling" of the tissue.

Finally, we list some of the assumptions used in the numerical modeling. First, our calculation of the tissue response is based on the rather limited available published experimental data for Arrhenius parameters that depend on the duration of exposure and type of the tissue. Additionally, coagulation depths were compared for various treatment modalities taking $\Omega(z) = 0.5$ as the coagulation criteria. However, when comparing coagulation depths it should be considered that different types of tissue damage might be encountered in the superficial layer even at the same coagulation depth. The comparison of the simulation with the reported coagulation depths is further complicated by the very gradual transition between the coagulated and normal collagen deeper in the dermis, and the arbitrary nature in determination of coagulation depths from histologic sections [19,72].

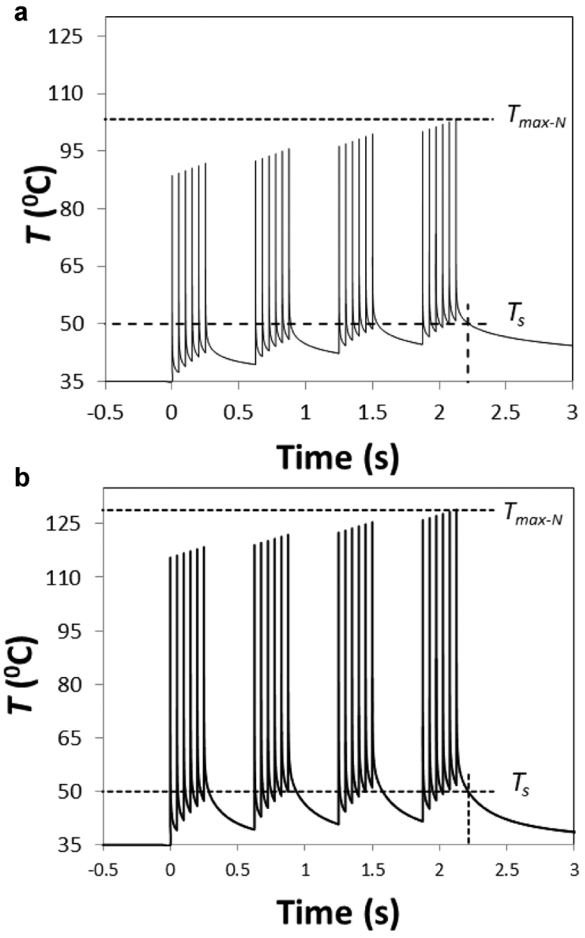

Fig. 9. Calculated temporal profile of the skin surface temperature during a sequence of four SMOOTH mode macro pulses each consisting of six micro pulses (resulting in $N = 4 \times 6 = 24$ micro pulses) for (**a**) $F_s = 4.9\,J/cm^2$ with a full-beam handpiece (R11 with 7 mm spot size); and (**b**) $F_s = 14.7\,J/cm^2$ with a patterned beam handpiece (PS03 with 0.85 mm micro spot size).

Furthermore, the level of superficial heat shock triggering was evaluated by assuming that the response to each laser pulse of a multiple-pulse exposure is independent of the response to other pulses. Generally, there is a cumulative effect in multiple-pulse exposures, as reflected, for example, by a reduction in the threshold energy per laser pulse relative to the single-pulse threshold in ocular damage studies [73]. However, the cumulative mechanism of multiple exposures is still not fully understood, and depends also on the type of tissue and irradiation [51,73].

A limitation of the study is also that the model did not include the effects of blood perfusion and tissue cooling as a result of natural convection. These effects could be of importance particularly for longer sequence irradiations lasting above about 10 seconds. However, since with these two cooling mechanisms being present the typical measured long-duration skin cooling times are on the order of

several minutes [72], and our temperature measurements for t_s up to 20 seconds are in rough agreement with the model predictions, we believe that these effects do not significantly affect the basic conclusions of the study.

Our simulations were made for skin parameters, and using the HPT data as obtained for the abdominal skin. However, in the case of moist oral and vaginal mucous tissue, evaporation of unbound water from the tissue during a single pulse and between pulses may decrease the temperature and as well the ablation threshold, tentatively explaining the observed difference in $\eta_s = \Delta T_s / F_s$, shown in Figure 5. In the model, it is assumed that the treated tissue is optically and physically homogeneous, which more closely applies to moist mucous tissues than to skin, where the water content has been found to vary considerably within the first approximately 50 μm of the epidermis [74].

A limitation of the study is also that the model did not include the effects of blood perfusion and tissue cooling as a result of natural convection. These effects could be of importance particularly for longer sequence irradiations lasting above about 10 seconds. However, since with these two cooling mechanisms being present the typical measured long-duration skin cooling times are on the order of several minutes [72], and our temperature measurements for t_s up to 20 s are in rough agreement with the model predictions, we believe that these effects do not significantly affect the basic conclusions of the study.

CONCLUSIONS

In conclusion, Er:YAG laser pulse stacking represents an example of complex thermal exposure dynamics during which the exposure times transition from extremely short to long durations. The tissue effects resulting from these dynamics were evaluated numerically using the VHS model, for two examples of non-ablative or minimally ablative Er:YAG laser pulse stacking treatments: (i) the "sub-resurfacing" performed at or near ablation laser fluences; and (ii) the "smooth-resurfacing" characterized by below-pain-threshold fluences.

Based on measurements on abdominal skin, the pain threshold temperature depends mainly on the long-exposure superficial skin temperature (T_s) by the end of the pulse sequence, and not on the peak skin temperatures (T_{max}) following individual laser pulses within the sequence.

The simulations show that for sub-resurfacing, the parameter range where no excessive damage to the tissue can occur is very narrow. On the other hand, using pain tolerance as an indicator, the smooth-resurfacing treatments can be performed more safely and without sacrificing the treatment efficacy.

Two preferred smooth-resurfacing treatment modalities were identified. One involves using optimally long pulse sequence durations with an optimal number of pulses, resulting in maximal short-exposure superficial tissue response, and moderate coagulation depths. And for deeper coagulation, without significant superficial heat shocking, very long pulse sequences with a large number of delivered pulses are to be used.

A comparison of the simulations with the established smooth-resurfacing clinical protocols in gynecology, ENT, and esthetics suggests that through clinical experience the clinical protocols have been optimized for the maximal superficial heat shock triggering effect.

Finally, further clinical research is needed to confirm the proposed role of superficial heat shocking in the reported smooth-resurfacing clinical results.

ACKNOWLEDGMENTS

This research was supported by the Ministry of Education, Science and Sport of Slovenia and the European Regional Development Fund (Project GOSTOP).

REFERENCES

1. Alster TS. Clinical and histologic evaluation of six erbium:YAG lasers for cutaneous resurfacing. Lasers Surg Med 1992;24:87–92.
2. Khatri KA, Ross V, Grevelink JM. Comparison of erbium:YAG and carbon dioxide lasers in resurfacing of facial rhytides. Arch Dermatol 1999;135(4):391–397.
3. Lukac M, Sult T, Sult R. New options and treatment strategies with the VSP erbium YAG aesthetics lasers. J Laser Health Acad 2007;2007(1/2):1–9.
4. Cole RP, Widdowson D, Moore JC. Outcome of erbium:yttrium aluminium garnet laser resurfacing treatments. Lasers Med Sci 2008;23(4):427–433.
5. Lukac M, Perhavec T, Nemes K, Ahcan U. Ablation and thermal depths in VSP Er:YAG laser skin resurfacing. J Laser Health Acad 2010; 2010(1);56-71.
6. Majaron B, Sustercic D, Lukac M, Skaleric U, Funduk N. Heat diffusion and debris screening in Er:YAG laser ablation of hard biological tissues. Appl Phys B Lasers Optics 1998;66:479–487.
7. Majaron B, Plestenjak P, Lukac M. Thermo-mechanical laser ablation of soft biological tissue: modeling the micro-explosions. Appl Phys B Lasers Optics 1999;69:71–80.
8. Fitzpatrick RE, Goldman MP, Sotur NM, Type WD. Pulsed carbon dioxide laser resurfacing of photoaged skin. Arch Dermatol 1996;132:395–402.
9. Greve B, Raulin C. Professional errors caused by laser and IPL technology in dermatology and aesthetic medicine. Preventive strategies and case studies. Derm Surg 2001;28:156–161.
10. Nanni CA, Alster TS. Complications of carbon dioxide laser resurfacing. An evaluation of 500 patients. Dermatol Surg 1998;24:315–320.
11. Majaron B, Srinivas SM, Huang HL, Nelson JS. Deep coagulation of dermal collagen with repetitive Er:YAG laser irradiation. Lasers Surg Med 2000;26:215–222.
12. Majaron B, Kelly KM, Park HB. Er:YAG laser skin resurfacing using repetitive long-pulse exposure and cryogen spray cooling: I. Histological study. Lasers Surg Med 2001;28:121–130.
13. Majaron B, Verkruysse W, Nelson S. Er:YAG laser skin resurfacing using repetitive long-pulse exposure and cryogen spray cooling: II. Theoretical analysis. Lasers Surg Med 2001;28:131–137.
14. Kunzi-Rapp K, Dierickx CC, Cambier B, Drosner M. Minimally invasive skin rejuvenation with Erbium: YAG laser used in thermal mode. Lasers Surg Med 2006;38 (10):899–907.
15. Drnovsek Olup B, Beltram M, Pizem J. Repetitive Er:YAG laser irradiation of human skin: A histological evaluation. Lasers Surg Med 2004;35:146–151.
16. Ross EV, McKinlay JR, Sajben FP, et al. Use of a novel Erbium laser in a Yucatan minipig: A study of residual

thermal damage, ablation, and would healing as a function of pulse duration. Lasers Surg Med 2002;30:93–100.
17. Alexiades-Armenakas MR, Dover JS, Arndt KA. The spectrum of laser skin resurfacing: Nonablative, fractional, and ablative laser resurfacing. J Am Acad Dermatol 2008;58(5):719–737.
18. Grema H, Greve B, Raulin C. Facial rhytides—Subsurfacing or resurfacing? A review. Lasers Surg Med 2003;32:405–412.
19. Lukac M, Zorman A, Bajd F. TightSculpting®: A complete minimally invasive body contouring solution; Part II: Tightening with FotonaSmooth® technology. J Laser Health Acad 2018;2018(1):126-35.
20. Lukac M, Gaspar A, Bajd F. Dual tissue regeneration: Nonablative resurfacing of soft tissues with FotonaSmooth® mode Er:YAG laser. J Laser Health Acad 2018;2018(1):1–15.
21. Fistonic N, Fistonic I, Findri Gustek S, et al. Minimally invasive, non-ablative Er:YAG laser treatment of stress urinary incontinence in women—A pilot study. Lasers Med Sci 2016;31:635–643.
22. Gaspar A, Brandi H. Non-ablative erbium YAG laser for the treatment of type III stress urinary incontinence (intrinsic sphincter deficiency). Laser Med Sci 2017;32(3):685–691.
23. Vizintin Z, Lukac M, Kazic M, Tettamanti M. Erbium laser in gynecology. Climacteric 2015;18(1):4–8.
24. Ogrinc UB, Sencar S, Lenasi H. Novel minimally invasive laser treatment of urinary incontinence in women. Lasers Surg Med 2015;47(9):689–697.
25. Mitsuyuki M, Stok U, Hreljac I, Yoda K, Vizintin Z. Treating vaginal laxity using nonablative Er:YAG laser: A retrospective case series of patients from 2.5 years of clinical practice. Sexual Med 2020;8:265–273.
26. Mija Blaganje M, Šćepanović, Žgur L, Verdenik I, Franja Pajk F, Lukanović A. Non-ablative Er:YAG laser therapy effect on stress urinary incontinence related to quality of life and sexual function: A randomized controlled trial. Eur J Obstet Gynecol Reprod Biol 2018;224:153–158.
27. Ebrahim HM, Gharib K. Correction of nasolabial folds wrinkle using intraoral non-ablative Er:YAG laser. J Cosmet Laser Ther 2018;20:364–368. https://doi.org/10.1080/14764172.2018.1439964
28. Quezada Gaón N, Binfa F. The effect of intraoral 2,940nm nonablative Erbium:YAG laser on the rejuvenation of the upper lip: A pilot study. Surg Cosmet Dermatol 2017;9(1):56–58.
29. Storchi IF, Parker S, Bovis F, Benedicenti S, Amaroli A. Outpatient erbium:YAG (2940 nm) laser treatment for snoring: A prospective study on 40 patients. Lasers Med Sci 2018;33(2):399–406.
30. Shiffman H, Lukac M. NightLase®: Minimally invasive laser-assisted uvulopalatoplasty. J Laser Health Acad 2018; 2018(1):39–44.
31. Neruntarat C, Khuancharee K, Shoowit P. Er:YAG laser for snoring: A systemic review and meta-analysis. Lasers Med Sci 2020;35(6):1231–1238.
32. Frelich H, Ścierski W, Marków M, Frelich J, Frelich H, Maciej M. Minimally invasive erbium laser treatment for selected snorers. Lasers Med Sci 2019;34(7):1413–1420.
33. Manstein D, Scott Herron G, Kehl Sink R, Tanner H, Anderson R. Fractional photothermolysis: A new concept for cutaneous remodeling using microscopic patterns of thermal injury. Lasers Surg Med 2004;34:426–438.
34. Tierney EP, Kouba DJ, Hanke CW. Review of fractional photothermolysis: Treatment indications and efficacy. Dermatol Surg 2009;35:1445–1461.
35. Gaspar A, Silva J, Calderon A, Di Placido V. Non-ablative resurfacing of mucosal tissue by SMOOTH-mode Er:YAG laser. 3rd LA&HA Super Symposium 2020. J Laser Health Acad 2020;2020(1):1–2.
36. Hympanova L, Mackova K, El-Domyati M, et al. Effects of non-ablative Er:YAG laser on the skin and the vaginal wall: Systematic review of the clinical and experimental literature. Int Urogynecol J 2020;31:2473–2484. https://doi.org/10.1007/s00192-020-04452-9
37. Lukac M, Lozar A, Perhavec T, Bajd F. Variable heat shock response model for medical laser procedures. Lasers Med Sci 2019;34(6):1147–1158.
38. Bowman PD. Survival of human epidermal keratinocytes after short-duration high temperature: Synthesis of HSP70 and IL-8. Am J Physiol 1997;272(6 Pt 1):C1988–C1994.
39. Capon A, Mordon S. Can thermal lasers promote skin wound healing? Am J Clin Dermatol 2003;4(1):1–12.
40. Mackanosa MA, Contag CH. Pulse duration determines levels of Hsp70 induction in tissues following laser irradiation. J Biomed Optics 2011;16(7):078002.
41. Lubart R, Friedmann H, Lavie R, Baruchin A. A novel explanation for the healing effect of the Er:YAG laser during skin rejuvenation. J Cosmet Laser Ther 2011;13:33–34.
42. Pearce J. Mathematical models of laser-induced tissue thermal damage. Int J Hyperth 2011;27(8):741–750.
43. Wright NT. On a relationship between the Arrhenius parameters from thermal damage studies. J Biomech Eng 2003;125(2):300–304.
44. Henriques FC, Moritz AR. Studies of thermal injury, 1. The conduction of heat to and through skin and the temperature attained therein. A theoretical and an experimental investigation. Am J Pathol 1947;23:531–549.
45. Moritz AR, Henriques FC. Studies of thermal injury, 2. The relative importance of time and surface temperature in the causation of burns. Am J Pathol 1947;23:695–720.
46. Simanovskii DM, Mackanos MA, Irani AR, et al. Cellular tolerance to pulsed hyperthermia. Phys Rev E 2006;74:011915.
47. Simanovskii D, Sarkar M, Irani A, et al. Cellular tolerance to pulsed heating. Proc. of SPIE 5695. 2005. pp 254–259. https://doi.org/10.1117/12.601774
48. Pirnat S, Lukac M, Ihan A. Thermal tolerance of *E. faecalis* to pulsed heating in the millisecond range. Lasers Med Sci 2011;26:229–237.
49. Lukac N, Tasic Muc B, Lukac M. High-temperature triggering of soft tissue regeneration by Er:YAG laser. 3rd LA&HA Super Symposium 2020. J Laser Health Acad 2020;2020(1):1–2.
50. Menendez AR, Cheney FE, Zuclich JA, Crump P. Probability-summation model of multiple laser-exposure effects. Health Phy 1993;65:523–528.
51. Lund BJ, Lund DJ, Edsall PR. Damage threshold from large retinal size repetitive-pulse laser exposures. Health Phys 2014;107(4):292–299.
52. Defrin R, Shachal-Shiffer M, Hadgadg M, Peretz C. Quantitative somatosensory testing of warm and heat-pain thresholds: The effect of body region and testing method. Clin J Pain 2006;22(2):130–136.
53. Yarnitsky D, Sprecher E, Zaslansky R, Hemli JA. Heat pain thresholds—Normative data and repeatability. Pain 1995;60(3):329–332.
54. Defrin R, Ohry A, Blumen N, Urca G. Sensory determinants of thermal pain. Brain 2002;125:501.
55. Arendt-Nielsen L, Chen C. Lasers and other thermal stimulators for activation of skin nociceptors in humans. Neurophysiol Clin 2003;33(6):259–268.
56. Green BG. Heat pain thresholds in the oral-facial region. Percept Psychophys 1985;38(2):110–114.
57. Lachenmeier DW, Lachenmeier W. Injury threshold of oral contact with hot foods and method for its sensory evaluation. Safety 2018;4:38.
58. Hardy LA, Chang C-H, Myers EM, Kennelly MJ, Fried NM. Laser treatment of female stress urinary incontinence: Optical, thermal, and tissue damage simulations. Proc SPIE Int Soc Opt Eng 2016;9689:96891R.
59. Bourke CD, Prendergast CT, Sanin DE, Oulton TE, Hall RJ, Mountford AP. Epidermal keratinocytes initiate wound healing and pro-inflammatory immune responses following percutaneous schistosome infection. Int J Parasitol 2015;45:215–224.
60. Pastar I, Stojadinovic O, Yin NC, et al. Epithelialization in wound healing: A comprehensive review. Adv Wound Care 2014;3(7):445–464.
61. Wojtowicz AM, Oliveira S, Carlson MW, Zawadzka A, Rousseau CF, Baksh D. The importance of both fibroblasts and keratinocytes in a bilayered living cellular construct used in wound healing. Wound Rep Reg 2014;22:246–255.
62. Lubart R, Kesler G, Lavie R, Friedmann H. Er:YAG laser promotes gingival wound repair by photo-dissociating water molecules. Photomed Laser Surg 2005;23(4):369–372.

63. Gordillo GM, Sen CK. Revisiting the essential role of oxygen in wound healing. Am J Surg 2003;186:259–263.
64. Rojkind M, Dominguez-Rosales JA, Nieto N, Green P. Role of hydrogen peroxide and oxidative stress in healing responses. Cell Mol Life Sci 2002;59:1872–1891.
65. Burdon RH. Superoxide and hydrogen peroxide in relation to mammalian cell proliferation. Free Radic Biol Med 1995;18:775–794.
66. Gill V. Hydrogen peroxide and the proliferation of BHK-21 cells. Free Radic Res 1995;23:471–486.
67. Carrasco E, Calvo MI, Blázquez-Castro A, et al. Photoactivation of ROS production in situ transiently activates cell proliferation in mouse skin and in the hair follicle stem cell niche promoting hair growth and wound healing. J Invest Dermatol 2015;135:2611–2622.
68. Ganceviciene R, Liakou AI, Theodoridis A, Makrantonaki E, Zouboulis CC. Skin anti-aging strategies. Dermatoendocrinol 2012;4(3):308–319.
69. Zhu H. Acupoints initiate the healing process. Med Acupunct 2014;26(5):264–270.
70. Liebla H, Kloth LC. Skin cell proliferation stimulated by microneedles. J Am Coll Clin Wound Spec 2013;4(1):2–6.
71. Ting Li T, Liao Q, Zhang H, Gao X, Li X, Zhang M. Anatomic distribution of nerves and microvascular density in the human anterior vaginal wall: Prospective study. PLOS One 2004;9(11):1–6.
72. Milanic M, Tasic B, Lukac N, Lukac M. Numerical study of hyper-thermic laser lipolysis with 1,064 nm Nd:YAG laser in human subjects. Lasers Surg Med 2019;51(10):897–909. https://doi.org/10.1002/lsm.23124
73. Griess GA, Blankenstein MF, Williford GG. Ocular damage from multiple-pulse laser exposures. Health Phys 1980; 39(6):921–927.
74. Noriaki Nakagawa N, Matsumoto M, Sakai S. In vivo measurement of the water content in the dermis by confocal Raman spectroscopy. Skin Res Technol 2010;16:137–141.